Optics Communications 281 (2008) 5360–5363

Contents lists available at ScienceDirect

Optics Communications

journal homepage: www.elsevier.com/locate/optcom

Confocal white light reflection imaging for characterization of metal nanostructures

C.L. Du, Y.M. You, J. Kasim, Z.H. Ni, T. Yu, C.P. Wong, H.M. Fan, Z.X. Shen *

Division of Physics and Applied Physics, School of Physical and Mathematical Sciences, Nanyang Technological University, 1 Nanyang Walk, Blk 5 Level 3, Singapore 637371, Singapore

ARTICLE INFO

Article history:
Received 23 April 2008
Received in revised form 14 July 2008
Accepted 25 July 2008

PACS:
78.67.−n
73.20.Mf

Keywords:
Localized surface plasmon (LSP)
Spatial resolution
Gold nanosphere
Silver nanowire

ABSTRACT

A simple far-field confocal white light reflection imaging system was proposed using a xenon (Xe) lamp as the incident light source. The best spatial resolution was determined to be about 410 nm. Localized surface plasmons (LSPs) of isolated single and dimer gold nanospheres were studied and the resonance energy difference between their LSPs was extracted. Polarization dependent reflection imaging and contrast spectrum of single silver nanowires were also investigated, which correlate closely with the polarization dependent excitation of their LSP.

1. Introduction

There is growing interest in the study of the optical properties of metal nanostructures as the resonant excitation of coherent electron oscillations (commonly known as localized surface plasmons, or LSPs) differ greatly from that of the bulk material and show wide applications [1–5]. Their size, shape and arrangement greatly affect the corresponding resonance energy of LSPs [6–7].

The ability to image metal nanostructures with a high spatial resolution as well as spectral resolution is very important for a host of studies both fundamental and practical. Specially, optical imaging and spectroscopic studies of individual metal nanoparticles and nanowires have attracted much attention recently [8–9]. Among them, scanning near-field optical microscopy (SNOM) has been widely adopted to study optical properties of metal nanostructures. It provides simultaneous topographical and optical information of the samples with high resolution. However, collecting an image by SNOM is very time-consuming and relies heavily on the equipment as well as the skill of the operator. It is also ill-suited for spectroscopic measurements due to the weak signals. Comparatively, far-field techniques are simpler and generate much stronger signals, which have been successfully used to study LSPs of gold nanoparticle arrays [10–11]. Moreover, far field white light scanning is a simple and low cost method, which also offers multiple-wavelength advantage and is suitable to study spectral properties. White light confocal scanning microscopy has also been used to characterize material morphology, refractive index profile of fibers, etc. [12,13], where aperture or fiber were used as confocal pinhole. To the best of our knowledge, there is no such report for individual metal nanostructures in literature by using confocal white light microscopy. The best spatial resolution for normal confocal white light (not including that from a super continuum light source [14]) scanning optical microscope has been improved from 1.5 μm to about 800 nm [13]. However, improvement of the spatial resolution is still much desired for the study of small-scale materials.

In this contribution, by decreasing the diameters of the incident light (aperture) and the collection fibers, the spatial resolution of the confocal reflection imaging was improved to be about 410 nm when Xe lamp was used as the light source. Individual single, dimer gold nanospheres and silver nanowires were scanned by the confocal system. Differences between the excitation of the LSPs of single and dimer spheres were revealed. Polarization dependent images of silver nanowires were discussed as well.

2. Experimental

Fig. 1 gives the schematic diagram of the experimental setup. A tunable aperture with a minimum diameter of 200 μm was introduced in the incident light path to enhance the spatial resolution. Light from a Xe lamp was polarized after passing through a polarizer. The incident light was focused onto the sample through a holographic beam splitter and an OLYMPUS microscope objective

* Corresponding author. Tel.: +65 63168855.
E-mail address: zexiang@ntu.edu.sg (Z.X. Shen).

0030-4018/$ - see front matter © 2008 Elsevier B.V. All rights reserved.
doi:10.1016/j.optcom.2008.07.078

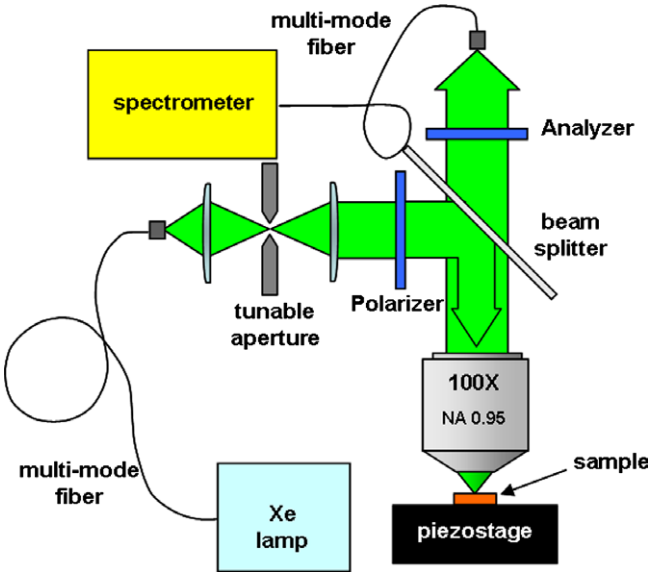

Fig. 1. Schematic diagram of the confocal white light reflection imaging system.

lens (100X, NA = 0.95). Samples were placed on a translation stage which provides coarse movement along the *x* and *y* axis, while the fine movement is offered by a piezostage with 100 μm travel distance along the *x* and *y* directions and 20 μm along the *z* direction. The piezostage also works as the mapping stage. The reflected light from the sample was collected by the same lens and directed to a spectrometer through a fiber. Fibers with various core diameters of 100, 50 and 25 μm were employed in this work. The collection fiber also works as a pinhole, which is confocal with the illuminating spot on the sample. The reflected light was directed to a 150 grooves/mm grating and detected by a TE-cooled charge-coupled device (CCD). Typical integration time for imaging was 100 ms/pixel. The stage movement and data acquisition were controlled using ScanCtrl Spectroscopy Plus software from WITec GmbH, Germany [15]. In a typical experiment, the sample is raster scanned point by point and a spectrum is collected for each point. Scanning electron microscope images were taken with field emission SEM (JEOL JSM-6700F).

Commercial gold nanospheres with a diameter of 50 nm deposited on 200 nm silicon dioxide films were used as samples for experiments. Silver nanowire samples with a diameter about 100 nm were fabricated by a simple hydrothermal method [16] and deposited onto silicon for use as well.

3. Results and discussion

The spatial resolution of the confocal reflection imaging system was determined by a scanning knife edge method [17] using a two-layer graphene sheet as the edge [18]. Table 1 lists the spatial resolution by using different diameter ($D2$) apertures and core diameter ($D1$) collection fibers. As shown, the spatial resolution becomes better with decreasing $D1$ and $D2$. The best resolution is revealed to be about 410 nm, obtained using the 25 μm core diameter collection fiber and setting the aperture diameter to 200 μm. This spatial resolution doubles the previously reported best spatial resolution (~800 nm) for white light scanning [13] and is even better than those of some laser scanning techniques [19,20]. This indicates that the aperture size, and especially the diameter of collection pinhole (the diameter of the collection fiber in our case), plays a very important role in improving the resolution. All the white light reflection images shown in this paper were obtained under this condition unless stated otherwise.

Table 1
Spatial resolution of the imaging system determined by knife-edge scanning method [17]

D_1	D_2		
	100 μm	50 μm	25 μm
1000 μm	0.805 ± 0.014 μm	0.652 ± 0.024 μm	0.434 ± 0.090 μm
200 μm	0.750 ± 0.016 μm	0.564 ± 0.016 μm	0.414 ± 0.080 μm

Gold nanospheres with diameter about 50 nm were studied, and their confocal white light reflection images were constructed by extracting light intensity from the corresponding reflection spectra for a selected wavelength range. The image at wavelength of 510–550 nm was shown in Fig. 2b as one example. As can be seen from the SEM image shown in Fig. 2a, it consists of three isolated single spheres and one dimer where the two spheres are almost in contact with each other. The four dark spots in Fig. 2b represent the images of the gold spheres, which correspond well to the SEM image. The size of the dark spots is measured to be 370–450 nm, approximating to the spatial resolution of the imaging system. Owing to the resolution limitation, it is reasonable that the white light reflection images can not distinguish between single and dimer spheres. If the collection fiber core diameter of 50 μm or 100 μm was used while the other experimental conditions were kept the same, the images from the spheres obviously overlap and the resolution is much worse than that with 25 μm fiber. As a comparison, the images employing the collection fiber with core diameter 100 μm were given in Fig. 2d. This confirms that we can achieve a higher spatial resolution by using a 25 μm core diameter collection fiber, in agreement with the edge fitting result in Table 1. It also demonstrates that to characterize metal nanostructures better with the system, the collection fiber with 25 μm core diameter is more favourable.

Once the positions of spheres are located, the contrast spectrum between the white light reflection intensity of the gold spheres and the substrate can be easily extracted, which is defined as

$$\text{Contrast} = (I_{\text{sample}} - I_{\text{substrate}})/I_{\text{substrate}} \quad (1)$$

where I_{sample} and $I_{\text{substrate}}$ refer to the white light reflection intensity of the sample and the substrate, respectively. Applying Eq. (1) to the single spheres, the obtained contrast spectra were plotted in Fig. 2c, which exhibits two dips (labeled **1** and **2**, respectively). For comparison, the contrast spectra for polarization of the incident light both parallel and perpendicular to the dimer axis were plotted in Fig. 2c as well. It is noticed that the position of dip 2 of isolated single spheres (at about 525 nm) coincides with that of the LSP of gold spheres with diameter 50 nm [21]. However, the same dip shows red shifts to 548 nm and 542 nm for the incident polarization parallel and perpendicular to the dimer axis, respectively. This is a result of the coupling effect between the two spheres of the dimer, in agreement with literature [22]. The larger red shift for the parallel polarization than that of the perpendicular case is understandable considering the stronger coupling of the dimer for parallel polarization. Fig. 2c also reveals that the position of the weak dip 1 for the single sphere almost overlaps with that of the dimer located at about 470 nm. This dip we believe to be originated from the multi-polar surface plasmon excitation of the gold spheres. Firstly, surface plasmon excitation at about 470 nm has been observed for gold nanospheres with diameters close to 40 nm, although it was ascribed to false spectral lines that arose from using a 488 nm argon laser [23]. Secondly, similar multi-polar surface plasmon excitation has been reported for other isolated metal nanoparticles [24]. Moreover, the excitation of LSPs leads to the enhancement of the absorption of the spheres, which consequently has the effect of reducing the reflection intensity [2], making the spheres dark in the corresponding images in Fig. 2b.

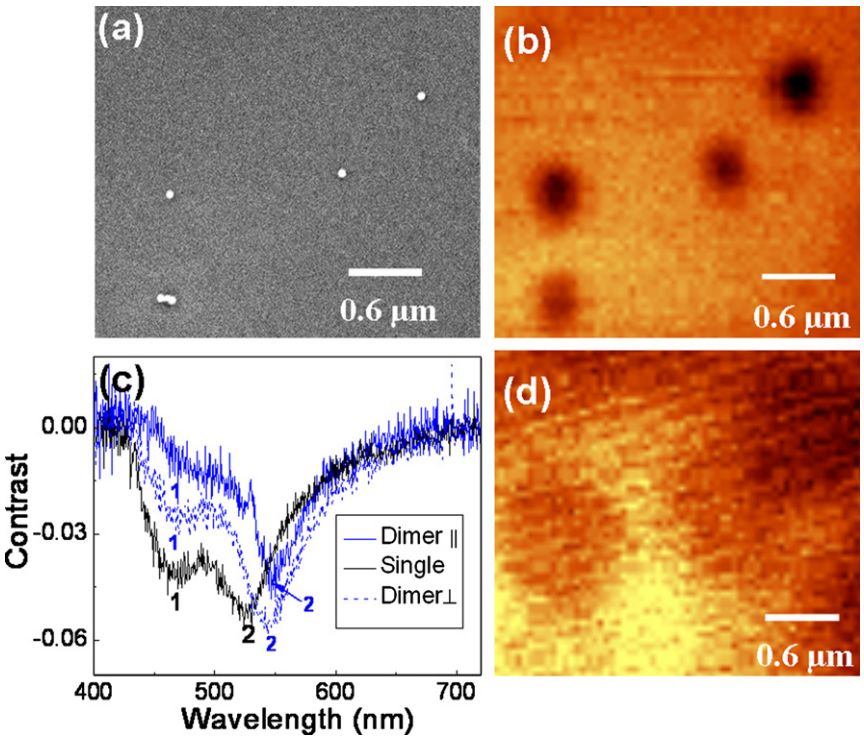

Fig. 2. SEM image (a) and confocal white light reflection images at wavelength 510–550 nm of gold nanospheres on 200 nm silicon dioxide films with collection fiber core diameter 25 μm (b) and 100 μm (d). (c), the contrast spectra for single (black lines) and dimer nanospheres for incident light parallel (solid lines) and perpendicular (dotted lines) to the dimer axis.

As another example, Fig. 3a and b shows the confocal white light reflection images of silver nanowires. Consider their wire-like shape; the polarization dependence of the white light imaging of Ag nanowires was investigated. The double-direction arrows in Fig. 3a and b indicates the polarization directions of the incident light. Under a reflection imaging system, silver nanowire is expected to be brighter than the substrate if only considering its larger reflectivity than that of the silicon substrate. However, Fig. 3a

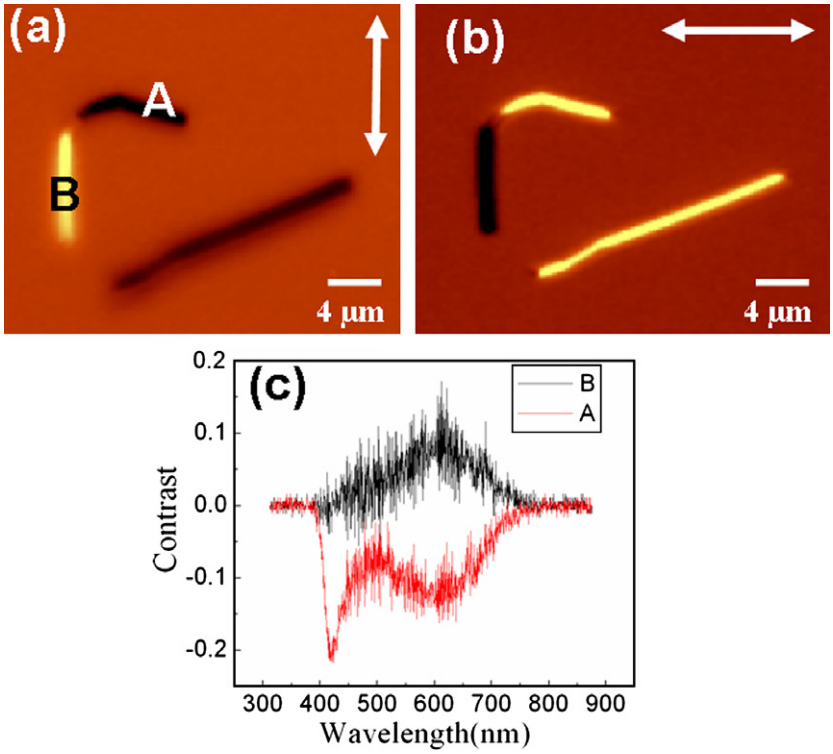

Fig. 3. The confocal white light reflection images (a,b) at wavelength 600–640 nm of silver nanowires on silicon substrate and their contrast spectra (c). The double-direction arrows in the figures indicate the polarization directions of the incident light while the letter A and B in (a) labels the position where the contrast spectrum is taken from.

shows that, different parts of the same bent nanowire exhibit different contrast compared to the substrate. The image contrast between the nanowire and the substrate also shows obvious polarization dependence. By rotating 90° of the incident polarization, their contrast reverses from comparison between Fig. 3a and b. This indicates that other mechanism also has contribution to the observed image contrast besides the different reflectivity information of the nanowire and the substrate. It is known that the excitation of LSPs of silver nanowires is anisotropic [25], which is sensitive to the polarization direction of the incident light. This can lead to the polarization dependence of the reflection images of Fig. 3, which also contribute to the different contrast for different parts of the same bent nanowire. Fig. 3c gives the contrast spectra of point A and point B as labeled in Fig. 3a compared to the substrate. When the nanowire axis is parallel to the incident light polarization (point B), a broad peak at 500–700 nm is observed, while when the nanowire axis is almost perpendicular to the incident light polarization (point A), two dips at about 420 nm and 500–700 nm, respectively, are detected. It is noticed that the positions for the broad peak and the broad dip at 500–700 nm coincide. As reported [26,27], for silver nanowires, the surface plasmon mode at around 500–700 nm experiences preferred excitation when the polarization of the incident light is parallel to the nanowire while the surface plasmon mode at 420 nm is dominant when the polarization of the incident light is perpendicular to the nanowire axis. Thus, the contrast spectra shown in Fig. 3c reveal the polarized behaviors of both surface plasmon modes. The images shown in Fig. 3a and b were extracted from the reflections in the range of 600–640 nm, which overlap with one of the surface plasmon modes (500–700 nm), their polarization dependence could be understood accordingly.

Finally, we would like to point out that the employed confocal imaging system is not limited to characterize individual metal nanostructures. It has also been successfully extended to the determination of the number of graphene layers and the extraction of their corresponding refractive index [18]. It can also be used to image other samples and structures, such as metal nanoarrays and biological specimen.

4. Conclusion

In conclusion, we have demonstrated that the spatial resolution of confocal white light reflection imaging could be significantly enhanced to be around 410 nm by combining a small aperture and a small collection fiber core diameter. Individual single, dimer gold nanospheres and silver nanowires were characterized by the imaging system. Apart from dipolar LSP, excitation of multi-polar LSP of gold nanospheres was also revealed. Compared to the resonance energy of single gold nanosphere, the resonance energy of the dimer is red-shifted due to the coupling between the two spheres in the dimer. The anisotropic excitation of LSP of a single silver nanowire was also observed, which contributes to the polarization dependent images besides their essential reflectivity difference from that of the substrate. As the white light imaging can be performed at different wavelengths, we expect interesting applications such as biomaterial mapping and plasmonic studies.

References

[1] S.R. Emory, W.E. Haskins, S. Nie, J. Am. Chem. Soc. 120 (1998) 8009.
[2] S. Kawata, Near-field Optics and Surface Plasmon Polaritons, Springer, 2001. 20.
[3] N. Grigorenko, A.K. Geim, H.F. Gleeson, Y. Zhang, A.A. Firsov, I.Y. Khrushchev, J. Petrovic, Nature (London) 438 (2005) 335.
[4] A.J. Haes, R.P.V. Duyne, J. Am. Chem. Soc. 124 (2002) 10596.
[5] J. Grand, M.L. Chapelle, J.L. Bijeon, P.M. Adam, A. Vial, P. Royer, Phys. Rev. B 72 (2005) 033407.
[6] L.J. Sherry, R. Jin, C.A. Mirkin, G.C. Schatz, R.P.V. Duyne, Nano Lett. 6 (2006) 2060.
[7] C. Noguez, J. Phys. Chem. C 111 (2007) 3806.
[8] B. Hecht, H. Bielefeldt, L. Novotny, Y. Inouye, D.W. Pohl, Phys. Rev. Lett. 77 (1996) 1889.
[9] J.K. Lim, K. Imura, T. Nagahara, S.K. Kim, H. Okamoto, Chem. Phys. Lett. 412 (2005) 41.
[10] G. Laurent, N. Félidj, S.L. Truong, J. Aubard, G. Lévi, J.R. Krenn, A. Hohenau, A. Leitner, F.R. Aussenegg, Nano Lett. 5 (2005) 253.
[11] G. Laurent, N. Félidj, J. Grand, J. Aubard, G. Lévi, A. Hohenau, F.R. Aussenegg, J.R. Krenn, Phy. Rev. B 73 (2006) 245417.
[12] A.C. Ribes, S. Damaskinos, A.E. Dixon, G.E. Carver, C. Peng, P.M. Fauchet, T.K. Sham, I. Coulthard, Appl. Phys. Lett. 66 (1995) 2321.
[13] Y.C. Youk, D.Y. Kim, Opt. Commun. 262 (2006) 206.
[14] K. Lindfors, T. Kalkbrenner, P. Stoller, V. Sandoghdar, Phys. Rev. Lett. 93 (2004) 037401.
[15] <http://www.witec.de/en/home/>.
[16] Z.H. Wang, J.W. Liu, X.Y. Chen, J.X. Wan, Y.T. Qian, Chem. Eur. J. 11 (2005) 160.
[17] G. Veshapidz, M.L. Trachy, M.H. Shah, B.D. Depaola, Appl. Opt. 45 (2006) 8197.
[18] Z.H. Ni, H.M. Wang, J. Kasim, H.M. Fan, T. Yu, Y.H. Wu, Y.P. Feng, Z.X. Shen, Nano Lett. 7 (2007) 2758.
[19] C. Rembe, A. Dräbenstedtb, Rev. Sci. Instrum. 77 (2006) 083702.
[20] L. Gütay, G.H. Bauer, Thin Solid Films 515 (2007) 6212.
[21] M.A. Dijk, M. Lippitz, M. Orrit, Acc. Chem. Res. 38 (2005) 594.
[22] A. Moores, F. Goettmann, New J. Chem. 30 (2006) 1121.
[23] S. Benrezzak, P.M. Adam, J.L. Bijeon, P. Royer, Surf. Sci. 491 (2001) 195.
[24] C. Beitia, Y. Borensztein, R. Lazzari, J. Nieto, R.G. Barrera, Phys. Rev. B 60 (1999) 6018.
[25] G. Schider, J.R. Krenn, A. Hohenau, H. Ditlbacher, A. Leitner, F.R. Aussenegg, W.L. Schaich, I. Puscasu, B. Monacelli, G. Boreman, Phys. Rev. B 68 (2003) 155427.
[26] A. Tao, F. Kim, C. Hess, J. Goldberger, R.R. He, Y.G. Sun, Y.N. Xia, P.D. Yang, Nano Lett. 9 (2003) 1229.
[27] P. Mohanty, I. Yoon, T. Kang, K.Y. Seo, K.S. Varadwaj, W.J. Choi, Q. H Park, J.P. Ahn, Y.D. Suh, H. Ihee, B. Kim, J. Am. Chem. Soc. 129 (2007) 9576.